Title

Integrated (epi)-Genomic Analyses Identify Subgroup-Specific Therapeutic Targets in CNS Rhabdoid Tumors

Journal

Cancer Cell, 30(6)

ISSN

1535-6108

Authors

Torchia, Jonathon
Golbourn, Brian
Feng, Shengrui
et al.

Publication Date

2016-12-01

DOI

10.1016/j.ccell.2016.11.003

Peer reviewed

HHS Public Access

Author manuscript

Cancer Cell. Author manuscript; available in PMC 2017 July 07.

Published in final edited form as:

Cancer Cell. 2016 December 12; 30(6): 891–908. doi:10.1016/j.ccell.2016.11.003.

Integrated (epi)-Genomic Analyses Identify Subgroup-Specific Therapeutic Targets in CNS Rhabdoid Tumors

A full list of authors and affiliations appears at the end of the article.

SUMMARY

We recently reported that atypical teratoid rhabdoid tumors (ATRTs) comprise at least two transcriptional subtypes with different clinical outcomes; however, the mechanisms underlying therapeutic heterogeneity remained unclear. In this study, we analyzed 191 primary ATRTs and 10 ATRT cell lines to define the genomic and epigenomic landscape of ATRTs and identify subgroup-specific therapeutic targets. We found ATRTs segregated into three epigenetic subgroups with distinct genomic profiles, SMARCB1 genotypes, and chromatin landscape that correlated with differential cellular responses to a panel of signaling and epigenetic inhibitors. Significantly, we discovered that differential methylation of a PDGFRB-associated enhancer confers specific sensitivity of group 2 ATRT cells to dasatinib and nilotinib, and suggest that these are promising therapies for this highly lethal ATRT subtype.

In Brief

Torchia et al. show that atypical teratoid rhabdoid tumors (ATRTs) are composed of three epigenetic subgroups that correlate with differential cellular responses to a panel of signaling and

*Correspondence: ddecarv@uhnresearch.ca (D.D.D.C.), james.rutka@sickkids.ca (J.T.R.), nada.jabado@mcgill.ca (N.J.), annie.huang@sickkids.ca (A.H.).

[73]Co-first author

[74]Lead Contact

ACCESSION NUMBERS

Data for whole-genome/exome DNA and RNA sequencing, ChIP sequencing for H3K27Ac, ATAC sequencing, gene expression, methylation and SNP genotyping array data have been deposited at the European Genome-Phenome Archive, EGA Study Accession ID EGAS00001000506.

SUPPLEMENTAL INFORMATION

Supplemental Information includes Supplemental Experimental Procedures, eight figures, and eight tables and can be found with this article online at http://dx.doi.org/10.1016/j.ccell.2016.11.003.

AUTHOR CONTRIBUTIONS

A.H., D.D.C., N.J., and J.T.R. conceived the projects. J.T. analyzed WGS/WES data assisted by L.L., M.B., S.M., A.V., B.G., M.D., P.S.C., and supervised by A.H., G.D.B., A.M., G.Bu., N.J., and M.Br. A.H. supervised RNA-seq analyses by J.T., D.M.G., and J.D.N.; gene expression and correlative analyses were carried out by J.T. with assistance from D.P. and G.D.B.; methylation data were collected by J.T. with assistance from D.P. and D.K.Q. ATAC and ChIP assays were performed by S.F., C.Z., K.C.H., T.M., and N.R.A. under supervision of D.D.C. Cellular, biochemical assays, and xenograft studies were performed by B.G., L.G., P.A., and K.C.H. with help from N.R.A., M.L., and M.Y. and supervised by A.H. A.C.P. performed 3C experiments supervised by D.D.C. J.T. performed analysis of ChIP and ATAC-seq data supervised by A.H. and D.D.C. in consultation with Ma.L. and P.G. Sequencing validation was performed under supervision of A.M., all other validation experiments were performed by B.G. and K.C.H. with assistance from T.S.C., A.N.R., and M.Y. under the supervision of A.H. and J.T.R. D.B., L.L.-C., Y.R., V.R., M.R., C.P.D., S.Y., H.-k.N., J.L., S.A., J.P., J.A.C., G.R.S., C.C.F., L.R., M.F., L.M.H., A.S.M., Y.W., S.A.C., J.R.H., D.C., D.K.B., N.F., D.S., A.K., M.G., P.H., T.H., L.B., B.W., J.H., A.C., T.E.V., E.I.H., S.C., H.N., H.T., I.F., H.D., D.F., T.W., C.F., D.D.E., K.S., D.J., J.M., S.Z., R.H., D.A.R., A.J..F., N.S., N.L., S.H., R.R.L., J.R.F., U.B., R.G., Da.M., U.S., T.N., T.T., J.Ph., J.Ma., S.Af., A.T.R., M.W.M., J.C.M., S.R., Y.G.G., M.D.T., U.T., T.P., A.R.J., E.B., S.K., A.E., P.D., and C.H.A. provided tumor materials/clinical data, and/or cell lines used in this study. Statistical analyses were performed by J.T. Histopathological analyses were performed by C.E.H. and M.Ba. J.T. and A.H. wrote the manuscript with input from B.G., D.D.C., N.J., and J.T.R.

epigenetic inhibitors. Specifically, dasatinib and nilotinib are identified as promising therapeutics for group 2 ATRTs.

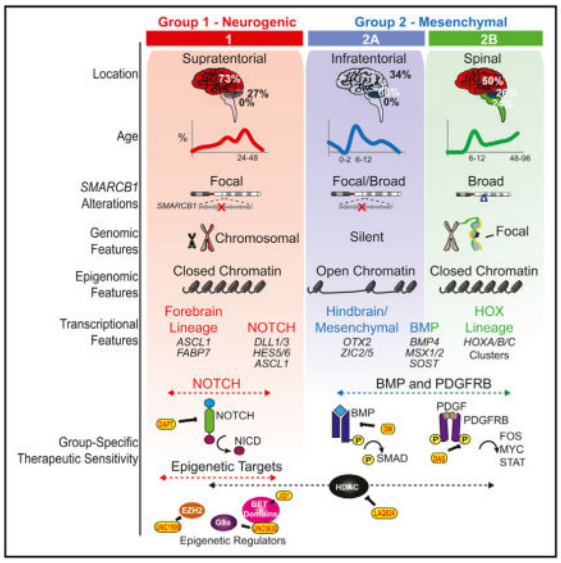

INTRODUCTION

Rhabdoid tumors (RT) are highly malignant, multi-lineage neoplasms of early childhood originally described in kidneys and soft tissues, but most frequently seen in the CNS where they are called atypical teratoid rhabdoid tumors (ATRTs). ATRTs were historically considered incurable, and although outcomes have improved with intensified multimodal therapy, most patients survive less than 1 year after diagnosis (Chi et al., 2008; Hilden, 2004; Lafay-Cousin et al., 2012; Tekautz, 2005).

Biallelic *SMARCB1* loss-of-function alterations are diagnostic of all RTs (Versteege et al., 1998). Up to 35% of ATRTs patients have heritable *SMARCB1* alterations, which predispose to multiple RTs (Eaton et al., 2011). Indeed, *Smarcb1*$^{+/-}$ mice also develop soft-tissue- or neural-crest-derived RTs (Klochendler-Yeivin et al., 2000; Roberts et al., 2002), and ATRTs can arise from conditional inactivation of *Smarcb1* (Han et al., 2016). SMARCB1 is a constitutive component of the SWI/SNF chromatin-remodeling complex, which exhibits substantial structural and functional diversity during neurogenesis. Loss of *SMARCA4* (Hasselblatt et al., 2011), which encodes another component of the SWI/SNF complex in some ATRTs, further underscores SWI/SNF-directed epigenetic mechanisms as critical in ATRT development. Although cumulative data support a central role for *SMARCB1* in RT initiation, specific mechanisms driving tumor development remain unclear. SMARCB1 deficiency leads to aberrant nucleosomal positioning by the SWI/SNF complex and is associated with upregulation of EZH2, a histone methyl transferase of the repressive PRC2 complex (Roberts and Orkin, 2004) with consequent deregulation of multiple downstream signaling pathways. These observations have led to RT therapies targeting EZH2 and other downstream pathways (Kim and Roberts, 2016; Wilson et al., 2010).

Surprisingly, despite the highly malignant and heterogeneous nature of ATRTs, exome studies indicate only recurrent *SMARCB1* coding alterations (Johann et al., 2016; Lee et al., 2012). We recently reported that ATRTs comprised at least two transcriptional subtypes with different clinical phenotypes (Torchia et al., 2015). While group 1 ATRTs with neurogenic signatures correlated with superior survival, group 2 ATRTs with mesenchymal signatures had aggressive, treatment-resistant phenotypes and dismal outcomes. However, mechanisms underlying varied therapeutic responses in ATRT patients remain unclear. Therefore, we performed an integrated genomic and functional epigenomic analysis of a large cohort of primary tumors and cell lines to elucidate subgroup-specific therapeutic sensitivities in ATRT.

RESULTS

ATRTs Comprise Three Epigenetic Subtypes with Distinct Clinical Profiles and Genotypes

We integrated whole-genome sequencing (WGS), whole-exome sequencing (WES), high-resolution copy number profiling, and RNA-sequencing (RNA-seq) analyses with gene expression and methylation profiling on a total of 191 primary tumors (Table S1). Consistent with prior studies, coding region single-nucleotide variation (SNV) rate was low with only recurrent *SMARCB1* coding mutations (Figure 1A, Table S2). However, intergenic mutation rate was significantly higher (0.64 mutation/Mb), suggesting that non-coding alterations may be important in ATRT (Figure 1A). Interestingly, we identified a spectrum of 379 copy number alterations (CNAs), including whole-arm gains and losses, focal deletions, duplications, and complex inter- and intrachromosomal gene rearrangements and uncovered 1.84–3.57 structural alterations/ATRT (Figure 1B; Tables S2 and S3). Cell adhesion, neural development, and chromatin-remodeling genes were targeted by recurrent coding region CNAs in up to 20% of ATRTs (Table S4) (Figure S1), and *SMARCB1* lacked previously reported mutational hotspots (Bourdeaut et al., 2011; Jackson et al., 2009). Notably, *SMARCB1* loss in 55.8% of ATRTs analyzed arose from structural events including exon duplications and gene fusions to *HOR-MAD2* and *GTPBP1* (Figures 1C–1E; Table S5), indicating structural alterations as predominant mechanisms for *SMARCB1* loss in ATRTs.

Unsupervised cluster analyses of 450k methylation micro-array data from 162 ATRTs revealed three epigenetic classes with high concordance to gene expression subtypes determined from 90 primary ATRTs (Figures 2A and 2B, S2A–S2E). While group 1 ATRTs comprised a single methylation cluster, group 2 tumors further segregated into two methylation subtypes (group 2A and 2B). ATRT subtypes correlated with distinct clinical and genotypic features (Figures 2C and 2D; Table S6); group 1 and 2A tumors arose predominantly in the supratentorial/cerebral (38/52; 73.1%) and infratentorial (cerebellum, brain stem) (42/64; 65.6%) locations, respectively. Group 1 and 2A ATRTs were seen in the oldest (median age 24 months; 95% confidence interval [CI] = 20.70–26.55) and youngest (median age 12 months; 95% CI = 11.05–13.00) children, respectively. Group 2B ATRTs encompassed more heterogeneous locations and included infra- (9/34; 26.5%), supratentorial (17/34; 50.0%), and all spinal (8/34; 23.5%) tumors. Group 2B patients spanned a broader age distribution and comprised the majority of patients older than 3 years of age (12/32; 37.5%). We found no significant subgroup association with gender or tumor metastases.

Although SNV alteration rates were comparable across subgroups, we observed genotypic differences; group 2B tumors had more focal genomic alterations (mean = 1.83; 95% CI = 1.43–2.31 alterations/tumor; p = 0.0024) than group 1 (mean = 0.86; 95% CI = 0.65–1.12 alterations/tumor) and 2A (mean = 0.88; 95% CI = 0.68–1.13 alterations/tumor; Figures 2C and Table S6) tumors. While group 1 tumors were distinguished by recurrent chr14 gains and chr19 losses, group 2B tumors exhibited focal copy number losses across multiple chromosomes, and group 2A ATRTs were genomically bland (Figure S3). Strikingly, our analyses revealed the type of genetic event leading to *SMARCB1* loss also differed between ATRT subgroups ($p = 2.79 \times 10^{-4}$; Figure 2C; Table S6). Most group 1 tumors (30/45; 66.7%) exhibited focal/subgenic alterations with predicted retention of the *SMARCB1* transcriptional start site; however, group 2B tumors had large deletions encompassing *SMARCB1* and frequently additional chr22 genes, thus indicating *SMARCB1*genotype:phenotype correlations in ATRTs.

ATRT Subgroups Have Distinct Lineage-Enriched Functional Genomes

Our observation of specific genotypes suggests that *SMARCB1* loss may have different functional consequences in ATRT subtypes. To define core molecular and cellular features of ATRT subgroups, we integrated supervised analyses of transcriptional and methylation data and observed that, while ATRTs generally exhibited a hypermethylated genome relative to other pediatric brain tumors, group 2A ATRTs had the lowest CpG island methylation levels compared with group 1 and 2B tumors (Figure S4A). Distribution of differentially methylated probes in CpG islands or gene bodies were similar across subgroups (Figure S4B); however, methylation and expression levels of lineage and developmental signaling genes differed significantly between subgroups (Figure 3A). These findings were corroborated by ingenuity pathway analyses (Figure 3B; Table S7), which revealed neurogenic genes (*FABP7*, *ASCL1*, *MYCN*, *c1orf61*) and genes involved in NOTCH (*DLL1/3 HES5/6*), glutamate receptor (*SLC17A8*, *SLC17A6*), and axonal guidance (*TUBB2B/3/4A*, *SEMA6A*) signaling, were most highly expressed and hypomethylated in group 1 ATRTs. BMP signaling (*BMP4*, *BAMBI*, *GDF5*, *FOXC1*) and mesenchymal differentiation (*SERPINF1*, *CLDN10*, *FBN2*, *MSX1*, *PDGFRB*) genes were most differentially expressed and methylated in group 2A/B tumors (Figure 3C; Table S7). Group 2A tumors were further distinguished by enrichment of visual cortex/hindbrain development (*OTX2*), retinol (*RBP1*, *RBP7*, *RDH5*, *RDH10*), and tyrosine (*TYR*) metabolism genes, while upregulation of *MYC* and *HOXB*/*C* clusters was seen in group 2B tumors (Figure 3C). Detailed analyses showed high concordance of CpG methylation patterns at promoters with ATRT subtypes, thus suggesting epigenetic regulation of developmental/cell lineage signaling pathways in ATRTs (Figures 3D and S5). Interestingly, while many group 2A enriched genes had functions in pluripotency and EMT, group 2B ATRTs exhibited heterogeneous profiles with enrichment of interferon signaling, cell adhesion, and cytoskeletal genes (Figure 3B).

To further investigate the distinct functional epigenome of ATRT subgroups, we performed high-resolution, genome-wide chromatin accessibility mapping using the assay for transposase-accessible chromatin (ATAC)-sequencing (ATAC-seq) analyses on five primary tumors (two group 1 and 2A, one group 2B) and four ATRT cell lines. In keeping with

methylation and transcriptional analyses, principle component and correlation analysis of primary ATRT ATAC-seq data showed segregation and association of ATRT subtypes with distinct ATAC-seq profiles (Figure 4A; Table S8). Integration of ATAC-seq footprints with RNA-seq data revealed open chromatin landscape in group 2A ATRTs that correlated with generally increased gene expression patterns in contrast to more closed chromatin landscapes and decreased gene expression patterns in group 1 tumors, while group 2B ATRTs exhibited an intermediate profile (Figure 4B). Specifically, we observed that group 1 (*ASCL1*, *FABP7*) and group 2A/B (*OTX2*, *ZIC1/4*, *ZIC5/2*) cell lineage genes and multiple signaling genes including ligands of NOTCH (*DLL1*, *HES6*) and BMP (*BMP4*, *MSX2*) pathways displayed open chromatin in a subtype-specific pattern. ATAC-seq analyses of ATRT cell lines showed similar patterns indicating that subgroup lineage and signaling features were maintained in cell lines (Figures 4C and 4D). These data suggest that ATRT subgroups and *SMARCB1* genotypes correlate with distinct functional epigenomes and indicate that epigenomic mechanisms drive lineage-specific gene expression and potential targetable therapeutic pathways in ATRTs.

NOTCH and BMP Signaling Drive ATRT Subgroup-Specific Cell Growth

To investigate subtype-specific therapies, we used expression profiling to determine molecular grouping of ten ATRT cell lines including 78C and 34C, respectively, derived from tumors T13 (group 1), T45 (group 2B), and established lines CHLA02, CHLA04, CHLA05, CHLA06, CHLA266, BT12, BT16, and SH. Prediction analysis of microarray (PAM) analyses of gene expression data from primary ATRTs reproducibly classified cell lines into subgroups 1 and 2 which, respectively, showed enrichment of neurogenic/NOTCH and mesenchymal/BMP signaling genes seen in corresponding primary ATRT subtypes. Western blot analyses confirmed expression of NOTCH intracellular domain (NICD) and phosphorylated SMAD1/5 (pSMAD1/5), respective effectors of NOTCH and BMP signaling in primary group 1 and 2 ATRTs and corresponding cell lines (Figure 5A), indicating that subtype signaling pathways were maintained.

To evaluate functional significance of NOTCH and BMP signaling, we used DAPT (N-[N-(3,5-difluorophenacetyl)-L-alanyl]-S-phenylglycine t-butyl ester), a γ-secretase inhibitor (Geling et al., 2002), and dorsomorphin (DM) (Yu et al., 2008) to, respectively, assess effects of NOTCH and BMP inhibition on a panel of group 1 (78C, CHLA05, CHLA02) and group 2A/B (SH, CHLA06, BT16) cell lines with most consistent growth phenotypes. Cell viability assays showed robust dose-dependent growth inhibition of group 1 and 2 cell lines with DAPT and DM treatment, respectively (Figures 5B and S6A), while cross-treatment of group 1 and 2 cell lines respectively with DM and DAPT had insignificant growth effects. Western blot and qRT-PCR analyses confirmed growth inhibition by DAPT correlated with dose-dependent downregulation of NICD and NOTCH transcriptional targets *HES1* and *HES5* in group 1 lines (Figures 5C and S6B). Similarly, we observed a dose-dependent decrease in pSMAD1/5 and BMP target genes *SOST* and *BAMBI* in group 2 cell lines (Figures 5D and S6B). Changes in NICD and pSMAD1/5 levels after DAPT and DM treatments also correlated with increased cell death in TUNEL assays (Figure S6C). We confirmed that the growth effects of γ-secretase inhibitors were mediated via NOTCH signaling in group 1 cells using siRNA-mediated knockdown of the NOTCH effector RBPJ,

which significantly diminished growth of group 1 (CHLA04/05) but not group 2 cell lines (BT12/BT16) (Figure 5E). These data collectively indicate that NOTCH and BMP are important ATRT subgroup-specific survival pathways and attractive pharmacologic targets.

Epigenetic Regulation of an Enhancer Element Underlies Group 2 ATRT Sensitivity to Pharmacologic Inhibitors of PDGFRB Signaling

Recent studies report promising therapies targeting various epigenetic and signaling pathways in ATRTs (Ginn and Gajjar, 2012); however, the relevance of these agents to ATRT subtypes is unknown as prior studies examined a few cell lines. To identify additional subgroup-specific targets, we tested the effects of 14 small molecules targeting epigenetic pathways on growth of three group 1 (CHLA04, 02, 05) and five group 2 ATRT (CHLA266/06, SH, BT16/12) lines (Figure S7A). We selected small-molecule inhibitors with well-defined in vitro cellular activity that target Bromo/BET domain proteins (JQ1, PFI-1,2 GSK2801, SGC-CBP30), methyltransferases (GSK343, UNC1999, UNC0642, UNC0638, A-366, J4, DOT1L, LLY507), and histone deacetylases (LAQ824). Cell viability assays showed that five of the 14 compounds had consistent significant effects on cell growth (>30% reduction in cell viability), including UNC0638, UNC1999, JQ1, LAQ824, and J4. LAQ824 and J4 significantly diminished growth of all cell lines. In contrast, UNC0638, UNC1999, and JQ1 treatment induced >30% reduction in viability of all three group 1 cell lines but did not affect three out of five group 2 cell lines (Figures 6A, 6B, S7A, and S7B). Interestingly, gene expression analyses showed that *EHMT2* (encodes G9a), *EZH2*, *BRD4*, and related loci (*BRD1-BRD7*) were highly expressed across all ATRTs (data not shown), and suggest that therapeutic sensitivity to epigenetic inhibitors may be dependent on a distinct functional chromatin landscape in ATRT subtypes.

Dasatinib and nilotinib are ATP-competitive small-molecule multi-tyrosine kinase inhibitors (TKIs) of BCR-ABL fusion protein, stem cell factor receptor, platelet-derived growth factor receptor (PDGFR), and Src family kinases (Rix et al., 2007). Both drugs are widely used in treatment of leukemia (Kantarjian et al., 2006) and some solid tumors (Araujo and Logothetis, 2010) but have not been extensively investigated in pediatric brain tumors. We therefore tested the sensitivity of ATRT cell lines to dasatinib and nilotinib as gene expression data indicated that *PDGFRB* was most differentially expressed between ATRT subgroups. In contrast to the relative insensitivity of group 2 ATRTs to epigenetic inhibitors, the growth of all five group 2 cell lines tested, including CHLA266 that was reported previously to be dasatinib sensitive (Kolb et al., 2008), was robustly diminished after dasatinib and nilotinib treatment (Figures 6A and 6B). Importantly, neither drug significantly affected the growth of group 1 cell lines. The well-characterized pharmacology of these drugs make them ideal candidates for clinical translation, hence we sought to further investigate the pharmacologic properties and mechanisms underlying the robust effect of both drugs on group 2 ATRT cell growth. Half-maximal inhibitory concentration (IC_{50}) assays revealed group 2 cell lines were up to 1,000 times more sensitive to dasatinib than group 1 cell lines (IC_{50} range 1.01 ± 0.02 to 5.23 ± 0.13 μM versus 3.98 ± 0.90 to 49.95 nM for group 1 and 2, respectively) (Figure 6C). As there are no reports of dasatinib efficacy in brain tumors, we tested dasatinib treatment in vivo using a BT16 orthotopic xenograft model which recapitulates classical rhabdoid morphology (Figure S7C) with predictable

engraftment rates. Mice with BT16 xenografts treated with daily intraperitoneal dasatinib (30 mg/kg) injections for 2 weeks had significantly prolonged survival compared with vehicle-treated controls (Figure 6D). Bioluminescence imaging (BLI) of a subset of tumor-bearing mice showed that drug treatment correlated significantly with decreased BLI signals ($p = 0.043$; Figure 6D).

To investigate mechanisms for dasatinib sensitivity, we compared expression of known dasatinib targets in ATRT subtypes. Integrated analyses identified *PDGFRB* as the most significantly differentially expressed locus in group 2 versus group 1 ATRTs (>2-fold change, $p = 6.35 \times 10^{-5}$) (Figure 6E), which was confirmed by western blot analyses of primary ATRTs (Figure 6F). *CSF1R*, which also encodes a potential dasatinib/nilotinib target and maps next to *PDGFRB*, was not differentially expressed or methylated in primary tumors or cell lines. These findings suggested that differential epigenetic regulation leading to *PDGFRB* upregulation may underlie the distinct sensitivity of group 2 cells to dasatinib and nilotinib. Consistent with high *PDGFRB* expression in group 2 ATRTs, ATAC-seq analyses revealed open chromatin at the *PDGFRB* but not the *CSF1R* promoter, specifically in group 2 primary tumors and cell lines (Figures 7A and 7B). Interestingly, ATAC-seq analyses also identified a distinct region of open chromatin in group 2 tumors and cell lines that corresponded to a potential regulatory domain 50 kb upstream of the *PDGFRB* promoter within exon 1 of *CSF1R* (chr5:149,491,285–149,493,716) (Figures 7A and 7B). To examine whether juxtaposition of the *PDGFRB* promoter and putative enhancer by chromatin looping underlies *PDGFRB* upregulation in group 2 ATRTs, we performed C3D analyses on primary tumor ATAC-seq data to evaluate the probability of peak associations (Thurman et al., 2012). The Pearson correlation co-efficient calculated for ATAC-seq peaks within a 500 kb window of the *PDGFRB* promoter showed significant correlations between the *PDGFRB* promoter and putative enhancer only in group 2 tumors, T26 (0.5170; $p < 0.0001$) and T27 (0.3028; $p = 0.0067$) (Figure 7C), and strongly supported direct interaction of the *PDGFRB* promoter and putative enhancer specifically in group 2 ATRTs. Detailed analyses of *CSF1R* and *PDGFRB* revealed hypomethylation of six CG residues within the putative enhancer in group 2 tumors and cell lines that correlated significantly with *PDGFRB* but not *CSF1R* expression (Figure 7D). Alignment with ENCODE data indicated features characteristic of enhancers in this region (Filippova et al., 1996; Malik et al., 2014), including differential H3KMe1, H3K4Me3, and H3K27Ac marks, and binding sites for multiple transcription factors including Myc network proteins, FOS and CTCF (Figures 7A and S8A). Together with the significant enrichment of *MYC* and *FOS* expression seen in group 2 ATRTs (Figure S8B), these findings suggest that differential epigenetic regulation of the putative enhancer underlies *PDGFRB* upregulation and distinct group 2 ATRT sensitivity to dasatinib and nilotinib. To confirm and map the putative *PDGFRB* enhancer, we performed H3K27Ac chromatin immunoprecipitation sequencing (ChIP-seq) on two dasatinib/nilotinib-resistant group 1 (CHLA04, 05) cell lines and a representative dasatinib/nilotinib-sensitive group 2 (BT12) cell line. Peak analyses showed that enriched H3K27Ac marks aligned with the predicted enhancer region only in group 2 lines, indicating enhancer activity only in group 2 ATRT cells (Figure 7B). 3C analyses revealed co-enrichment of probes mapping to the *PDGFRB* enhancer and promoter regions in BT12 and CHLA05 cells (Figure 8A). Of note, a second peak in the *PDGFRB* gene body was not associated with

H3K27Ac enrichment in BT12 cells. Taken together with the enrichment of H3K27Ac marks at the putative *PDGFRB* enhancer in BT12 but not CHLA04 and 05 cells, these data indicate that direct interaction of a distant active enhancer and promoter via chromatin looping facilitates *PDGRB* expression in group 2 ATRT cells (Figure 8B). Consistent with these observations, western blot analyses showed high phospho-PDGFRB (pPDGFRB) expression in group 2, but not group 1 ATRT cell lines (Figure 8C), and robust downregulation of pPDGFRB after dasatinib treatment in group 2 cells (Figure 8D). Collectively, our results suggest that epigenetic regulation via differential methylation of a *PDGFRB*-associated enhancer specifically drives the sensitivity of group 2 ATRTs to small-molecule inhibitors of the *PDGFRB* signaling axis and indicate that dasatinib/nilotinib are important agents for the particularly lethal group 2 ATRTs.

DISCUSSION

ATRTs are highly malignant cancers with substantial heterogeneity in disease presentation and poorly defined biology for which best therapeutic approaches are undefined. Here, we demonstrate that ATRTs comprise three epigenetic subtypes that correlate with distinct tumor locations, patient age, lineage-enriched methylation and transcriptional signatures, and unique global and *SMARCB1*-specific genotypes. Our data reveal that ATRT subgroups are associated with a distinct epigenomic landscape and sensitivity to inhibitors of NOTCH, BMP, PDGFRB, and epigenetic signaling. Significantly, we discovered that differential methylation of a *PDGFRB* enhancer underlies the robust and distinct sensitivity of group 2 ATRTs to dasatinib and nilotinib, two well-characterized and widely used cancer drugs.

Cumulative studies indicate that a convergence of epigenomic features reflecting cellular origins and specific somatic alterations underlies diverse tumor phenotypes (Feinberg et al., 2006). Here, we observed that ATRTs segregate into subtypes with specific lineage-enriched methylation signatures, distinct tumor location, and age of presentation suggestive of origins from different neural progenitors. In the predominantly supratentorial group 1 ATRTs, we observed distinct methylation and enrichment of neurogenic loci including forebrain markers *LHX2* (Roy et al., 2014) and *MEIS2* (Cecconi et al., 1997), as well as *FABP7* and *ASCL1*, markers of radial glial neural progenitors (Anthony et al., 2004), indicating these as potential cell of origins for group 1 ATRTs. In contrast, differentially methylated and expressed loci in group 2 ATRTs were primarily mesenchymal lineage/signaling (*BMP/PDGFRB*) and mid/hindbrain development (*ZIC1*, *-2*, *-4*, *-5*, *OTX2*, *HOXB/C*) genes and suggest that group 2A/B ATRTs, which are primarily infratentorial and spinal tumors, develop from mid/hindbrain neural progenitors. Enrichment of neuronal development pathways in group 1 tumors contrasted with a dominance of stem cell differentiation and pluripotency pathways in group 2A ATRTs. We also observed that, in contrast to group 1 and 2B, group 2A tumors were associated with global CpG island hypomethylation, a more open chromatin landscape and overall increased gene expression patterns reminiscent of more primitive cell types. These data further suggest that group 2A tumors, which arise in the youngest patients (12.00 months 95% CI = 11.05–13.00), originate from highly primitive neural precursors. Our findings corroborate a recent study that also reported three epigenetic subtypes of ATRTs with distinct enhancer landscapes (Johann et al., 2016), and a study of murine ATRTs derived from a conditional ROSA-Cre model (Han et al., 2016). Our data revealed that

ATRTs have rare coding mutations but exhibit subtype-enriched patterns of CNAs and *SMARCB1* genotypes, and suggest different mechanisms of tumor initiation and progression in ATRT subtypes. Notably *SMARCB1* deletions in group 2B ATRTs were frequently accompanied by copy number-driven gene expression changes in candidate modifier loci with neurogenic and epigenetic functions, including *BCR*, *MKL*, and *EP300* (Kaartinen et al., 2001).

As ATRTs lack other recurrent coding alterations, there has been substantial interest in epigenetic therapies for ATRTs. Specifically, promising studies of EZH2 (Knutson et al., 2013) and BET domain (Tang et al., 2014) inhibitors have been reported. Intriguingly, while our screen of small epigenetic inhibitors confirmed the therapeutic effects of UNC1999 and JQ1, respectively EZH2 and BET domain inhibitors, we observed growth inhibitory effects predominantly in group 1 lines. Similarly, we observed that only group 1 lines were sensitive to UNC0638, a chemical compound for histone methyl transferase G9a, while LAQ824, a histone acetylase inhibitor, diminished growth in all cell lines. These findings may reflect more general epigenetic functions of histone deacetylases versus histone methyl transferases. Interestingly, the cellular responses to epigenetic compounds overlapped with the sensitivity to inhibitors of NOTCH and BMP signaling pathways, critical mediators of lineage-specific progenitor cell survival (Ericson et al., 1998). Specifically, group 1 cells with neurogenic transcriptional and epigenomic profiles were sensitive to DAPT, UNC0638, and UNC1999, while group 2 cell lines with limited features of neural differentiation were largely insensitive to these three inhibitors. In contrast, we observed a distinct sensitivity of group 2 cell lines to inhibitors of BMP and PDGFRB, both mediators of mesenchymal signaling. Of note, recent reports indicate a functional and physical interaction of the G9a/GLP and polycomb repressive complex 2 (PRC2) epigenetic silencing machineries and co-regulation of neuronal developmental genes by G9a and PRC2 (Mozzetta et al., 2014). These observations collectively indicate that lineage-associated epigenomic landscapes of ATRTs have critical implications for the development of ATRT subtype-specific therapies. Future investigations to define contributions of other epigenetic modifiers implicated by our genomic and experimental data will clearly be important for informing the development of ATRT therapies.

Our data extend an earlier report of PDGFRA/B expression in some ATRTs and rhabdoid tumor sensitivity to TKIs (Koos et al., 2010). Here, we observed that nilotinib and dasatinib have growth inhibitory effects only in group 2 ATRT cells, including the CHLA266 cell line reported previously to be dasatinib sensitive (Kolb et al., 2008). Importantly, our studies show that dasatinib significantly prolongs the survival of mice with orthotopic group 2 ATRT xenografts, thus indicating that dasatinib can accumulate at a sufficient concentration for tyrosine kinase inhibition in brain tumors. Our studies also suggest that PDGFRB expression is a promising biomarker for dasatinib sensitivity in ATRTs. These findings have significant implications for ATRT treatment as the safety and efficacy of dasatinib are established in adults and children. Interestingly, consistent with the reported enrichment of BMP signaling/mesenchymal lineage genes in non-CNS RTs (Birks et al., 2011; Chun et al., 2016; Gadd et al., 2010), we observed an overlap in the methylation profiles of non-CNS RTs and group 2 ATRTs (data not shown), which suggests that some group 2 ATRTs and non-CNS tumors characteristically seen in very young children with rhabdoid predisposition

syndrome, may have common or closely related cellular origins. Indeed, we observed that dasatinib and nilotinib also robustly inhibited the growth of G401, a renal RT cell line (data not shown) and suggest potential roles for dasatinib and nilotinib in non-CNS RT treatment.

Despite evidence of a critical etiologic role for *SMARCB1* in RT initiation, the pathobiology of ATRTs remains poorly elucidated. Our data suggest that *SMARCB1* loss via diverse mechanisms in different cellular contexts, together with additional epigenetic and genetic events, underlies the clinical heterogeneity of human ATRTs. These observations have significant implications for the fundamental understanding and targeting of SWI/SNF function in neoplastic growth and clinical management of ATRTs. Specifically, our analyses, which reveal a spectrum of alterations throughout *SMARCB1*, indicate that current diagnostic methods may underestimate the frequency of *SMARCB1* alterations in ATRTs. We have identified known and potential drugs and drug-like inhibitors with different therapeutic effects in molecular subtypes of ATRTs. In addition to nominating dasatinib and nilotinib as promising repurposed drugs for ATRTs, our comprehensive characterization of ATRT cell lines provides a rich resource for the further development of other candidate ATRT drugs. Most importantly, our study underscores the significant limitations of current chemoradiotherapeutic regimens used uniformly for all ATRT patients. Together with our earlier observations that indicate differential outcomes for molecular subtypes of ATRTs, our study provides a critical framework for informing pre-clinical studies as well as risk- and biology-stratified clinical trials for ATRTs.

EXPERIMENTAL PROCEDURES

Tumor and Patient Information

All tumors and clinical information were collected through an international collaborative network (see Supplemental Experimental Procedures) with consent as per protocols approved by the Hospital Research Ethics Board at participating institutions. In total, 194 CNS (191 primary and 3 recurrent) and 9 non-CNS RT samples were collected for genomic analyses (Table S3). All ATRTs were diagnosed according to the World Health Organization CNS tumor classification criteria (Louis and Wiestler, 2007) and confirmed by BAF47 immunostains (BD Biosciences, catalog no. 612110). Biallelic *SMARCB1* alterations were confirmed using FISH, MLPA, targeted exons 1–9 Sanger sequencing, or WGS/WES analyses. DNA or RNA from snap frozen tumor were investigated with one or more of WGS/WES, RNA-seq and high-resolution copy number/SNP, gene expression, and methylation array analyses; 123 samples with DNA from formalin-fixed, paraffin-embedded materials were analyzed with the Illumina 450k methylation arrays. Animal studies were conducted in accordance with the policies and regulations for ethical treatment of animals approved for the Toronto Center for Phenogenomics.

Statistical Analyses

Difference in nucleotide transition/transversion rates from WGS SNV calls were determined using the two-proportion Z test with Yates' correction for continuity. Significance of differences in gender, location, metastasis, and individual genomic loci between ATRT subgroups were analyzed using a two-sided Fisher's exact test. The Kruskal-Wallis test was

used to assess the significance of tumor subgroups in relation to age and counts of genomic alterations. Student's t test and the Mann-Whitney-Wilcoxon test with false discovery rate (FDR) correction were used, respectively, to test for differences in gene expression and methylation between groups. All analyses were conducted in the R statistical environment (v2.15.2) or with SPSS version 22.0. A p value of <0.05 was regarded as significant for all analyses.

Supplementary Material

Refer to Web version on PubMed Central for supplementary material.

Authors

Jonathon Torchia[1,2,7,13,73], Brian Golbourn[1,8,13,73], Shengrui Feng[3,14,73], King Ching Ho[7,13,73], Patrick Sin-Chan[1,2,7,13], Alexandre Vasiljevic[15], Joseph D. Norman[7,13], Paul Guilhamon[14], Livia Garzia[10,13], Natalia R. Agamez[7,13], Mei Lu[7,13], Tiffany S. Chan[1,2,7,13], Daniel Picard[7,13], Pasqualino de Antonellis[10,13], Dong-Anh Khuong-Quang[16,17], Aline C. Planello[14], Constanze Zeller[14], Dalia Barsyte-Lovejoy[14], Lucie Lafay-Cousin[20], Louis Letourneau[19], Mathieu Bourgey[19], Man Yu[13], Deena M.A. Gendoo[7,13], Misko Dzamba[5], Mark Barszczyk[13], Tiago Medina[14], Alexandra N. Riemenschneider[8,13], A. Sorana Morrissy[10,13], Young-Shin Ra[22], Vijay Ramaswamy[7,13], Marc Remke[7,13], Christopher P. Dunham[23], Stephen Yip[25], Ho-keung Ng[26], Jian-Qiang Lu[27], Vivek Mehta[28], Steffen Albrecht[18], Jose Pimentel[30], Jennifer A. Chan[21], Gino R. Somers[12], Claudia C. Faria[31], Lucia Roque[32], Maryam Fouladi[33], Lindsey M. Hoffman[34], Andrew S. Moore[35], Yin Wang[36], Seung Ah Choi[37], Jordan R. Hansford[38], Daniel Catchpoole[39], Diane K. Birks[34], Nicholas K. Foreman[34], Doug Strother[29], Almos Klekner[40], Laszló Bognár[40], Miklós Garami[41], Péter Hauser[41], Tibor Hortobágyi[42], Beverly Wilson[29], Juliette Hukin[24], Anne-Sophie Carret[43], Timothy E. Van Meter[44], Eugene I. Hwang[45], Amar Gajjar[46], Shih-Hwa Chiou[47], Hideo Nakamura[48], Helen Toledano[49], Iris Fried[50], Daniel Fults[51], Takafumi Wataya[52], Chris Fryer[24], David D. Eisenstat[29], Katrin Scheinemann[53], Adam J. Fleming[53], Donna L. Johnston[54], Jean Michaud[55], Shayna Zelcer[56], Robert Hammond[57], Samina Afzal[58], David A. Ramsay[57], Nongnuch Sirachainan[59], Suradej Hongeng[59], Noppadol Larbcharoensub[60], Richard G. Grundy[61], Rishi R. Lulla[62], Jason R. Fangusaro[62], Harriet Druker[7], Ute Bartels[7], Ronald Grant[7], David Malkin[2,7,11], C. Jane McGlade[3,13], Theodore Nicolaides[63], Tarik Tihan[64], Joanna Phillips[64], Jacek Majewski[17,19], Alexandre Montpetit[19], Guillaume Bourque[17,19], Gary D. Bader[4], Alyssa T. Reddy[65], G. Yancey Gillespie[66], Monika Warmuth-Metz[67], Stefan Rutkowski[68], Uri Tabori[1,7,11,13], Mathieu Lupien[3,14], Michael Brudno[5,11], Ulrich Schüller[69], Torsten Pietsch[70], Alexander R. Judkins[71], Cynthia E. Hawkins[1,9,13], Eric Bouffet[7,13], Seung-Ki Kim[37], Peter B. Dirks[8,13], Michael D. Taylor[8,10,13], Anat Erdreich-Epstein[72], Cheryl H. Arrowsmith[14], Daniel D. De Carvalho[3,14,*], James T. Rutka[6,8,13,*], Nada Jabado[16,17,*], and Annie Huang[1,2,7,13,74,*]

Affiliations

[1]Department of Laboratory Medicine and Pathobiology, University of Toronto, Toronto, ON M5G0A4, Canada [2]Department of Paediatrics, University of Toronto, Toronto, ON M5G0A4, Canada [3]Department of Medical Biophysics, University of Toronto, Toronto, ON M5G0A4, Canada [4]Department of Molecular Genetics, University of Toronto, Toronto, ON M5G0A4, Canada [5]Department of Computer Science, University of Toronto, Toronto, ON M5G0A4, Canada [6]Department of Surgery, University of Toronto, Toronto, ON M5G0A4, Canada [7]Division of Hematology/Oncology, Hospital for Sick Children, Toronto, ON M5G1X8, Canada [8]Division of Neurosurgery, Hospital for Sick Children, Toronto, ON M5G1X8, Canada [9]Division of Pathology, Hospital for Sick Children, Toronto, ON M5G1X8, Canada [10]Program in Developmental & Stem Cell Biology, Hospital for Sick Children, Toronto, ON M5G1X8, Canada [11]Program in Genetics & Genome Biology, Hospital for Sick Children, Toronto, ON M5G1X8, Canada [12]Department of Paediatric Laboratory Medicine, Hospital for Sick Children, Toronto, ON M5G1X8, Canada [13]Arthur and Sonia Labatt Brain Tumour Research Centre, Hospital for Sick Children, Toronto, ON M5G1X8, Canada [14]Princess Margaret Cancer Center, University Health Network, Toronto, ON M5G1L7, Canada [15]Department of Pathology, Groupement Hospitalier Est, CHU de Lyon, Lyon-Bron 69677, France [16]Department of Pediatrics, McGill University, Montreal, QC H3Z2Z3, Canada [17]Department of Human Genetics, McGill University, Montreal, QC H3Z2Z3, Canada [18]Department of Pathology, McGill University, Montreal, QC H3Z2Z3, Canada [19]Genome Quebec Innovation Centre, McGill University, Montreal, QC H3A1A4, Canada [20]Division of Pediatric Hematology/Oncology, Alberta Children's Hospital, AB T3B6A8, Canada [21]Department of Pathology and Laboratory Medicine, University of Calgary, Calgary, AB T2N1N4, Canada [22]Department of Neurosurgery, Asan Medical Center, Seoul 138-736, Korea [23]Division of Anatomic Pathology, Children's and Women's Health Centre of B.C, University of British Columbia, Vancouver, BC V6H3N1, Canada [24]Division of Hematology and Oncology, Children's and Women's Health Centre of B.C, University of British Columbia, Vancouver, BC V6H3N1, Canada [25]Department of Pathology & Laboratory Medicine, University of British Columbia, V6T1Z3, Canada [26]Department of Anatomical and Cellular Pathology, Chinese University of Hong Kong, Hong Kong, China [27]Laboratory Medicine and Pathology, Stollery Children's Hospital, University of Alberta, Edmonton, AB T2W3N2, Canada [28]Division of Neurosurgery, Stollery Children's Hospital, University of Alberta, Edmonton, AB T2W3N2, Canada [29]Division of Pediatric Hematology/Oncology, Stollery Children's Hospital, University of Alberta, Edmonton, AB T2W3N2, Canada [30]Divison of Pathology, Hospital de Santa Maria, Centro Hospitalar Lisboa Norte, Lisbon 1649-035, Portugal [31]Department of Neurosurgery, Hospital de Santa Maria, Centro Hospitalar Lisboa Norte, Lisbon 1649-035, Portugal [32]Cytometry and Cytogenetic Laboratory, CIPM, Portuguese Cancer Institute, Lisbon 1099-023, Portugal [33]Division of Oncology, Department of Cancer and Blood Diseases, Cincinnati Children's Hospital, Cincinnati, OH 45229, USA [34]Department of Pediatrics, University of Colorado,

Denver, CO 80045, USA [35]Oncology Service, Children's Health Queensland Hospital; University of Queensland Diamantina Institute, Brisbane, QLD 4102, Australia [36]Research Institute of Health Development Strategies, Fudan University, Shanghai 200032, China [37]Division of Pediatric Neurosurgery, Seoul National University Children's Hospital, Seoul 03080, Korea [38]Royal Children's Hospital, Murdoch Children's Research Institute, Melbourne, VIC 3052, Australia [39]Children's Cancer Research Unit, Children's Hospital at Westmead, Westmead, NSW 2145, Australia [40]Department of Neurosurgery, University of Debrecen, Debrecen 4032, Hungary [41]Second Department of Pediatrics, Semmelweis University, Budapest 1094, Hungary [42]Department of Histopathology, University of Szeged, Szeged 6720, Hungary [43]Department of Pediatrics, Division of Hematology-Oncology, Université de Montréal/CHU Sainte-Justine, Montreal, QC H3T1C5, Canada [44]Department of Neurosurgery, Virginia Commonwealth University, Richmond, VA 23298-0631, USA [45]Department of Oncology, Children's National Medical Center, Washington, DC 20010, USA [46]Division of Neuro-Oncology, St. Jude Children's Research Hospital, Memphis, TN 38105, USA [47]Department of Medical Research, Taipei Veterans General Hospital and National Yang-Ming University, Taipei 112, Taiwan [48]Department of Neurosurgery, Kumamoto University, Kumamoto 860-8556, Japan [49]Department of Pediatric Hematology Oncology, Children's Medical Center of Israel, Petach Tikva 49202, Isreal [50]Department of Pediatric Hematology-Oncology, Hadassah Hebrew University Medical Center, Jerusalem 91120, Israel [51]Department of Neurosurgery, University of Utah, School of Medicine, Salt Lake City, UT 84132, USA [52]Department of Neurosurgery, Shizuoka Children's Hospital, Shizuoka 420-8660, Japan [53]Department of Pediatrics, McMaster University, Hamilton, ON L8S4K1, Canada [54]Department of Pediatrics, Children's Hospital of Eastern Ontario, University of Ottawa, Ottawa, ON K1H8L1, Canada [55]Pathology and Laboratory Medicine, Children's Hospital of Eastern Ontario, University of Ottawa, Ottawa, ON K1H8L1, Canada [56]Division of Pediatric Hematology/Oncology, Children's Hospital, London Health Sciences Center, London, ON N6A5A5, Canada [57]Department of Pathology and Laboratory Medicine, Children's Hospital of Western Ontario, University of Western Ontario, London, ON N6A5W9, Canada [58]Department of Pediatrics, Dalhousie University, Halifax, NS B3H4R2, Canada [59]Department of Pediatrics, Faculty of Medicine, Ramathibodi Hospital, Mahidol University, Bangkok 10300, Thailand [60]Department of Pathology, Faculty of Medicine, Ramathibodi Hospital, Mahidol University, Bangkok 10400, Thailand [61]Children's Brain Tumour Research Centre, University of Nottingham, Nottingham NG72RD, England [62]Division of Pediatric Hematology-Oncology and Stem Cell Transplantation, Ann and Robert H. Lurie Children's Hospital of Chicago, Chicago, IL 60611, USA [63]Department of Pediatrics (Hematology/Oncology), University of California, San Francisco, San Francisco, CA 94143-0112, USA [64]Department of Neurosurgery, University of California, San Francisco, San Francisco, CA 94143-0112, USA [65]Department of Pediatric Hematology and Oncology, University of Alabama, Birmingham, AL 35233, USA [66]Department of Neurosurgery, University of Alabama, Birmingham, AL 35233, USA [67]Department of Neuroradiology,

University of Würzburg, Würzburg 97070, Germany [68]Department of Pediatric Hematology and Oncology, University Medical Center Hamburg-Eppendorf, Hamburg 20246, Germany [69]Department of Neuropathology, University Medical Center Hamburg-Eppendorf, Hamburg 20246, Germany [70]Institute for Neuropathology, University of Bonn Medical Center, Bonn 53105, Germany [71]Department of Pathology & Laboratory Medicine, Children's Hospital of Los Angeles, Los Angeles, CA 90027, USA [72]Department of Pediatrics, Children's Hospital Los Angeles, Keck School of Medicine, University of Southern California, Los Angeles, CA 90027, USA

Acknowledgments

This work was supported by funds from Genome Canada, 110814 (A.H. and N.J.), CCSRI #703279 (A.H. and D.D.C.), b.r.a.i.n.child, Mitchell Duckman, Tal Doron, and Suri Boon foundations (A.H. and J.T.R.) and C17 Childhood Cancer and Blood Disorders Research Network (L.L.C., E.B., A.H.). J.T. and P.S.C. are Ontario Graduate Scholars; D.G. and J.D.N. are, respectively, Brain Canada and CIHR Research Fellows. Technical support from V. Lau, A. Ma, and staff of the McGill University and Génome Québec Innovation Center, the Princess Margaret Genomics Center, the Center for Applied Genomics Toronto, the Rare Brain Tumor Consortium (http://www.rarebraintumorconsortium.ca), tumor banks of contributing centers (Table S8), and tissue contributions from Dr. A. Korshunov are gratefully acknowledged.

References

Anthony TE, Klein C, Fishell G, Heintz N. Radial glia serve as neuronal progenitors in all regions of the central nervous system. Neuron. 2004; 41:881–890. [PubMed: 15046721]

Araujo J, Logothetis C. Dasatinib: a potent SRC inhibitor in clinical development for the treatment of solid tumors. Cancer Treat Rev. 2010; 36:492–500. [PubMed: 20226597]

Birks DK, Donson AM, Patel PR, Dunham C, Muscat A, Algar EM, Ashley DM, Kleinschmidt-Demasters BK, Vibhakar R, Handler MH, Foreman NK. High expression of BMP pathway genes distinguishes a subset of atypical teratoid/rhabdoid tumors associated with shorter survival. Neurooncol. 2011; 13:1296–1307.

Bourdeaut F, Lequin D, Brugieres L, Reynaud S, Dufour C, Doz F, Andre N, Stephan JL, Perel Y, Oberlin O, et al. Frequent hSNF5/INI1 germ-line mutations in patients with rhabdoid tumor. Clin Cancer Res. 2011; 17:31–38. [PubMed: 21208904]

Cecconi F, Proetzel G, Alvarez-Bolado G, Jay D, Gruss P. Expression of Meis2, a Knotted-related murine homeobox gene, indicates a role in the differentiation of the forebrain and the somitic mesoderm. Dev Dyn. 1997; 210:184–190. [PubMed: 9337138]

Chi SN, Zimmerman MA, Yao X, Cohen KJ, Burger P, Biegel JA, Rorke-Adams LB, Fisher MJ, Janss A, Mazewski C, et al. Intensive multimodality treatment for children with newly diagnosed CNS atypical teratoid rhabdoid tumor. J Clin Oncol. 2009; 27:385–389. [PubMed: 19064966]

Chun HJ, Lim EL, Heravi-Moussavi A, Saberi S, Mungall KL, Bilenky M, Carles A, Tse K, Shlafman I, Zhu K, et al. Genome-wide profiles of extra-cranial malignant rhabdoid tumors reveal heterogeneity and dysregulated developmental pathways. Cancer Cell. 2016; 29:394–406. [PubMed: 26977886]

Eaton KW, Tooke LS, Wainwright LM, Judkins AR, Biegel JA. Spectrum of SMARCB1/INI1 mutations in familial and sporadic rhabdoid tumors. Pediatr Blood Cancer. 2011; 56:7–15. [PubMed: 21108436]

Ericson J, Norlin S, Jessell TM, Edlund T. Integrated FGF and BMP signaling controls the progression of progenitor cell differentiation and the emergence of pattern in the embryonic anterior pituitary. Development. 1998; 125:1005–1015. [PubMed: 9463347]

Feinberg AP, Ohlsson R, Henikoff S. The epigenetic progenitor origin of human cancer. Nat Rev Genet. 2006; 7:21–33. [PubMed: 16369569]

Filippova GN, Fagerlie S, Klenova EM, Myers C, Dehner Y, Goodwin G, Neiman PE, Collins SJ, Lobanenkov VV. An exceptionally conserved transcriptional repressor, CTCF, employs different combinations of zinc fingers to bind diverged promoter sequences of avian and mammalian c-myc oncogenes. Mol Cell Biol. 1996; 16:2802–2813. [PubMed: 8649389]

Gadd S, Sredni ST, Huang CC, Perlman EJ. Group, Renal Tumor Committee of the Children's Oncology Group. Rhabdoid tumor: gene expression clues to pathogenesis and potential therapeutic targets. Lab Invest. 2010; 90:724–738. [PubMed: 20212451]

Geling A, Steiner H, Willem M, Bally-Cuif L, Haass C. A gamma-secretase inhibitor blocks Notch signaling in vivo and causes a severe neurogenic phenotype in zebrafish. EMBO Rep. 2002; 3:688–694. [PubMed: 12101103]

Ginn KF, Gajjar A. Atypical teratoid rhabdoid tumor: current therapy and future directions. Front Oncol. 2012; 2:114. [PubMed: 22988546]

Han ZY, Richer W, Freneaux P, Chauvin C, Lucchesi C, Guillemot D, Grison C, Lequin D, Pierron G, Masliah-Planchon J, et al. The occurrence of intracranial rhabdoid tumours in mice depends on temporal control of Smarcb1 inactivation. Nat Commun. 2016; 7:10421. [PubMed: 26818002]

Hasselblatt M, Gesk S, Oyen F, Rossi S, Viscardi E, Giangaspero F, Giannini C, Judkins AR, Fruhwald MC, Obser T, et al. Nonsense mutation and inactivation of SMARCA4 (BRG1) in an atypical teratoid/rhabdoid tumor showing retained SMARCB1 (INI1) expression. Am J Surg Pathol. 2011; 35:933–935. [PubMed: 21566516]

Hilden JM. Central nervous system atypical teratoid/rhabdoid tumor: results of therapy in children enrolled in a registry. J Clin Oncol. 2004; 22:2877–2884. [PubMed: 15254056]

Jackson EM, Sievert AJ, Gai X, Hakonarson H, Judkins AR, Tooke L, Perin JC, Xie H, Shaikh TH, Biegel JA. Genomic analysis using high-density single nucleotide polymorphism-based oligonucleotide arrays and multiplex ligation-dependent probe amplification provides a comprehensive analysis of INI1/SMARCB1 in malignant rhabdoid tumors. Clin Cancer Res. 2009; 15:1923–1930. [PubMed: 19276269]

Johann PD, Erkek S, Zapatka M, Kerl K, Buchhalter I, Hovestadt V, Jones DT, Sturm D, Hermann C, Segura Wang M, et al. Atypical teratoid/rhabdoid tumors are comprised of three epigenetic subgroups with distinct enhancer landscapes. Cancer Cell. 2016; 29:379–393. [PubMed: 26923874]

Kaartinen V, Gonzalez-Gomez I, Voncken JW, Haataja L, Faure E, Nagy A, Groffen J, Heisterkamp N. Abnormal function of astroglia lacking Abr and Bcr RacGAPs. Development. 2001; 128:4217–4227. [PubMed: 11684658]

Kantarjian H, Giles F, Wunderle L, Bhalla K, O'Brien S, Wassmann B, Tanaka C, Manley P, Rae P, Mietlowski W, et al. Nilotinib in imatinib-resistant CML and Philadelphia chromosome-positive ALL. N Engl J Med. 2006; 354:2542–2551. [PubMed: 16775235]

Kim KH, Roberts CW. Targeting EZH2 in cancer. Nat Med. 2016; 22:128–134. [PubMed: 26845405]

Klochendler-Yeivin A, Fiette L, Barra J, Muchardt C, Babinet C, Yaniv M. The murine SNF5/INI1 chromatin remodeling factor is essential for embryonic development and tumor suppression. EMBO Rep. 2000; 1:500–506. [PubMed: 11263494]

Knutson SK, Warholic NM, Wigle TJ, Klaus CR, Allain CJ, Raimondi A, Porter Scott M, Chesworth R, Moyer MP, Copeland RA, et al. Durable tumor regression in genetically altered malignant rhabdoid tumors by inhibition of methyltransferase EZH2. Proc Natl Acad Sci USA. 2013; 110:7922–7927. [PubMed: 23620515]

Kolb EA, Gorlick R, Houghton PJ, Morton CL, Lock RB, Tajbakhsh M, Reynolds CP, Maris JM, Keir ST, Billups CA, Smith MA. Initial testing of dasatinib by the pediatric preclinical testing program. Pediatr Blood Cancer. 2008; 50:1198–1206. [PubMed: 17914733]

Koos B, Jeibmann A, Lunenburger H, Mertsch S, Nupponen NN, Roselli A, Leuschner I, Paulus W, Fruhwald MC, Hasselblatt M. The tyrosine kinase c-Abl promotes proliferation and is expressed in atypical teratoid and malignant rhabdoid tumors. Cancer. 2010; 116:5075–5081. [PubMed: 20629032]

Lafay-Cousin L, Hawkins C, Carret AS, Johnston D, Zelcer S, Wilson B, Jabado N, Scheinemann K, Eisenstat D, Fryer C, et al. Central nervous system atypical teratoid rhabdoid tumours: the

Canadian Paediatric Brain Tumour Consortium experience. Eur J Cancer. 2012; 48:353–359. [PubMed: 22023887]

Lee RS, Stewart C, Carter SL, Ambrogio L, Cibulskis K, Sougnez C, Lawrence MS, Auclair D, Mora J, Golub TR, et al. A remarkably simple genome underlies highly malignant pediatric rhabdoid cancers. J Clin Invest. 2012; 122:2983–2988. [PubMed: 22797305]

Louis, DN., Wiestler, OD. WHO Classification of Tumours of the Central Nervous System, Fourth Edition (IARC). 2007.

Malik AN, Vierbuchen T, Hemberg M, Rubin AA, Ling E, Couch CH, Stroud H, Spiegel I, Farh KK, Harmin DA, Greenberg ME. Genome-wide identification and characterization of functional neuronal activity-dependent enhancers. Nat Neurosci. 2014; 17:1330–1339. [PubMed: 25195102]

Mozzetta C, Pontis J, Fritsch L, Robin P, Portoso M, Proux C, Margueron R, Ait-Si-Ali S. The histone H3 lysine 9 methyltransferases G9a and GLP regulate polycomb repressive complex 2-mediated gene silencing. Mol Cell. 2014; 53:277–289. [PubMed: 24389103]

Rix U, Hantschel O, Durnberger G, Remsing Rix LL, Planyavsky M, Fernbach NV, Kaupe I, Bennett KL, Valent P, et al. Chemical proteomic profiles of the BCR-ABL inhibitors imatinib, nilotinib, and dasatinib reveal novel kinase and nonkinase targets. Blood. 2007; 110:4055–4063. [PubMed: 17720881]

Roberts CW, Orkin SH. The SWI/SNF complex–chromatin and cancer. Nat Rev Cancer. 2004; 4:133–142. [PubMed: 14964309]

Roberts CW, Leroux MM, Fleming MD, Orkin SH. Highly penetrant, rapid tumorigenesis through conditional inversion of the tumor suppressor gene Snf5. Cancer Cell. 2002; 2:415–425. [PubMed: 12450796]

Roy A, Gonzalez-Gomez M, Pierani A, Meyer G, Tole S. Lhx2 regulates the development of the forebrain hem system. Cereb Cortex. 2014; 24:1361–1372. [PubMed: 23307637]

Tang Y, Gholamin S, Schubert S, Willardson MI, Lee A, Bandopadhayay P, Bergthold G, Masoud S, Nguyen B, Vue N, et al. Epigenetic targeting of Hedgehog pathway transcriptional output through BET bromodomain inhibition. Nat Med. 2014; 20:732–740. [PubMed: 24973920]

Tekautz TM. Atypical teratoid/rhabdoid tumors (ATRT): improved survival in children 3 years of age and older with radiation therapy and high-dose alkylator-based chemotherapy. J Clin Oncol. 2005; 23:1491–1499. [PubMed: 15735125]

Thurman RE, Rynes E, Humbert R, Vierstra J, Maurano MT, Haugen E, Sheffield NC, Stergachis AB, Wang H, Vernot B, et al. The accessible chromatin landscape of the human genome. Nature. 2012; 489:75–82. [PubMed: 22955617]

Torchia J, Picard D, Lafay-Cousin L, Hawkins CE, Kim SK, Letourneau L, Ra YS, Ho KC, Chan TS, Sin-Chan P, et al. Molecular subgroups of atypical teratoid rhabdoid tumours in children: an integrated genomic and clinicopathological analysis. Lancet Oncol. 2015; 16:569–582. [PubMed: 25882982]

Versteege I, Sévenet N, Lange J, Rousseau-Merck MF, Ambros P, Handgretinger R, Aurias A, Delattre O. Truncating mutations of hSNF5/INI1 in aggressive paediatric cancer. Nature. 1998; 394:203–206. [PubMed: 9671307]

Wilson BG, Wang X, Shen X, McKenna ES, Lemieux ME, Cho YJ, Koellhoffer EC, Pomeroy SL, Orkin SH, Roberts CWM. Epigenetic antagonism between polycomb and SWI/SNF complexes during oncogenic transformation. Cancer Cell. 2010; 18:316–328. [PubMed: 20951942]

Yu PB, Hong CC, Sachidanandan C, Babitt JL, Deng DY, Hoyng SA, Lin HY, Bloch KD, Peterson RT. Dorsomorphin inhibits BMP signals required for embryogenesis and iron metabolism. Nat Chem Biol. 2008; 4:33–41. [PubMed: 18026094]

Significance

ATRTs are considered to be genetically homogeneous with bland genomes. Our integrated genomic studies indicate a higher non-coding mutation rate and predominantly structural coding alterations, which suggest a more complex ATRT genome. We identify three epigenetic ATRT subtypes associated with distinct genotypic, chromatin, and functional landscapes that correlate with cellular responses to various signaling and epigenetic pathway inhibitors. Significantly, we identify two well-characterized cancer drugs, dasatinib and nilotinib, as promising therapeutic agents for group 2 ATRTs. Together with our earlier findings, our data provide compelling rationale for the development of a risk- and biology-stratified trial for ATRTs.

Highlights

- ATRTs comprise three molecular and epigenetic subgroups: group 1, 2A, and 2B
- Distinct chromatin landscape drives subgroup-specific lineage and signaling features
- ATRT subgroups exhibit distinct sensitivity to signaling and epigenetic inhibitors
- Epigenetically regulated PDGFRB enhancer drives TKI sensitivity in group 2 ATRTs

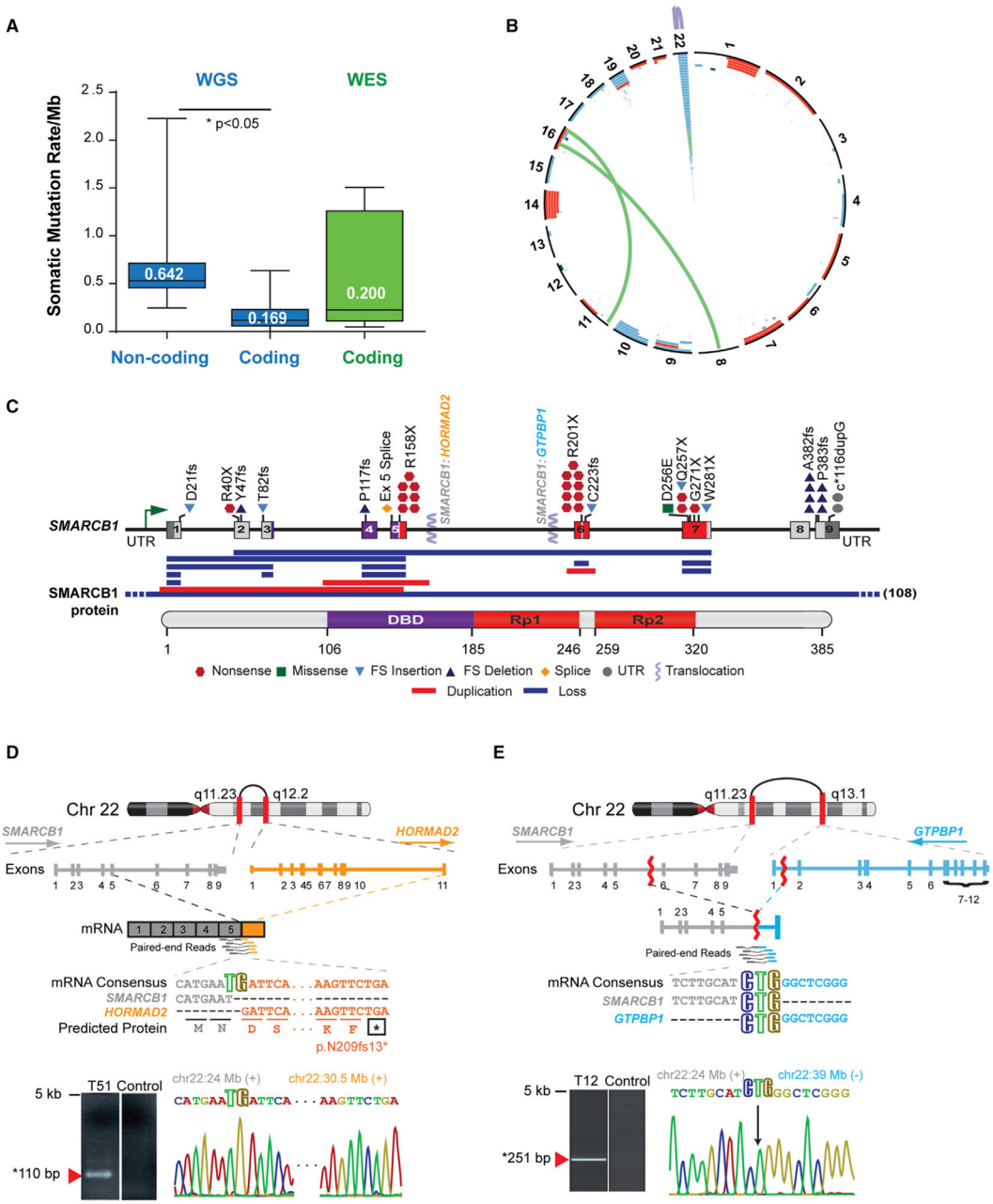

Figure 1. ATRT Coding Genome Is Predominantly Targeted By Structural Alterations

(A) Global genome and coding region somatic mutation rate in ATRTs. Median somatic mutation rates/Mb were calculated using WGS and WES data on 26 primary ATRTs with matched normal DNA. Boxplot middle represents median, box boundaries represent first and third quartiles; whiskers represent min and max values.

(B) Circos plot of recurrent structural alterations, including SCNAs and gene rearrangements, from integrated WGS, RNA-seq, SNP, and 450k methylation array copy number data of 180 primary ATRTs.

(C) Schema of *SMARCB1* alterations relative to DNA binding domain (DBD) and repeat regions 1 and 2 (Rp1 and Rp2) domains in the SMARCB1 protein.
(D) Schema of a chr22q intrachromosomal fusion of *SMARCB1* exon 5 (gray) and *HORMAD2* exon 11 (orange) identified by RNA-seq in ATRT T51 with consensus sequence and RT-PCR and Sanger sequencing validation of the fusion mRNA.
(E) Schematic of a chr22q intrachromosomal translocation involving *SMARCB1* intron 5 (gray) and *GTPBP1* intron 1 (blue) identified by WES in ATRT T12 with CREST predicted mRNA consensus sequence of respective gene fragments and PCR and Sanger sequencing validation of breakpoint.
See also Figure S1, Tables S1, S2, S3, S4, and S5.

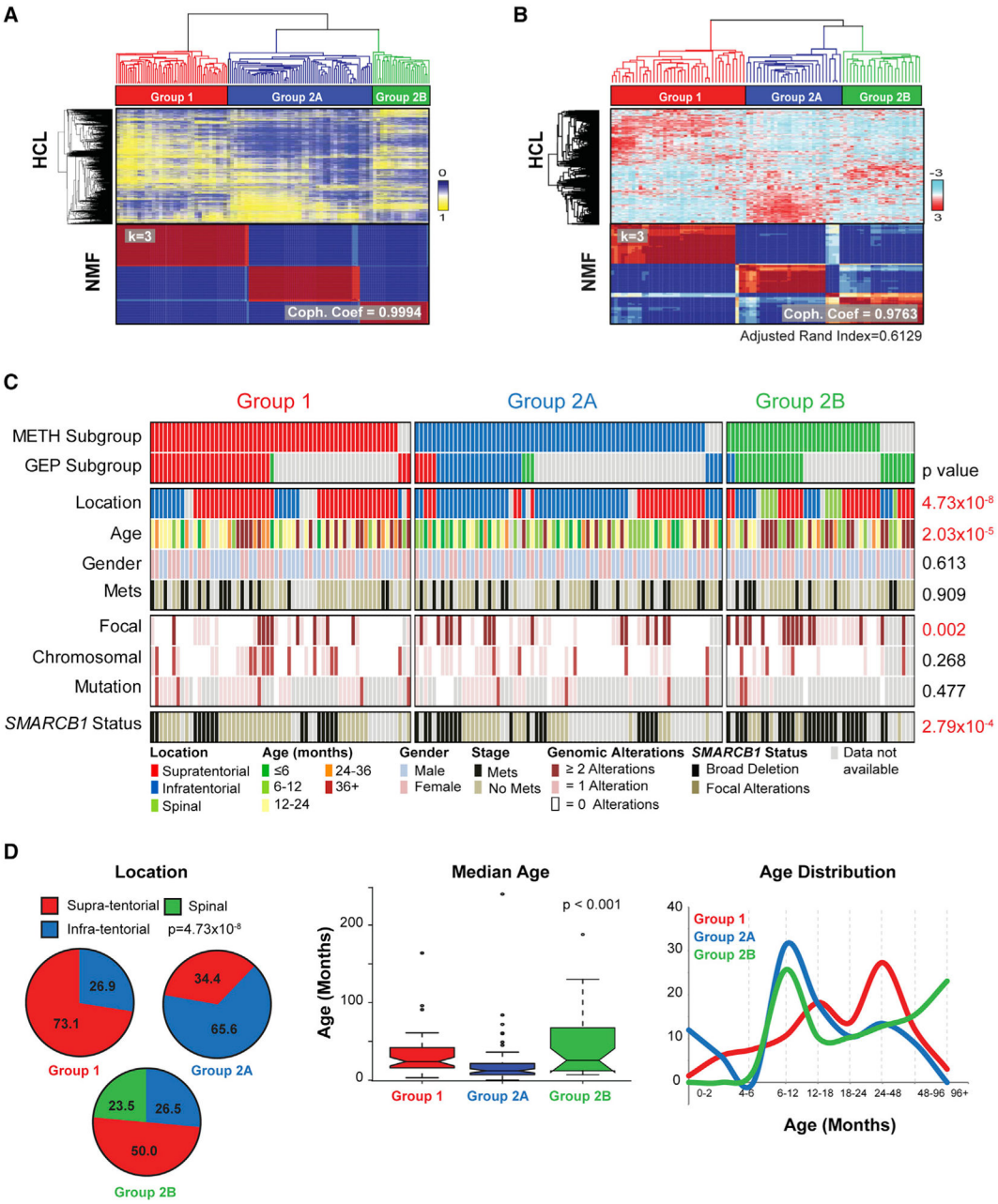

Figure 2. ATRTs Comprise Three Epigenetic Subgroups with Distinct Clinical Profiles and Genotypes

(A and B) ATRTs were classified by unsupervised consensus hierarchical (HCL) and non-negative matrix factorization (NMF) cluster analyses of 450k methylation array (A) or Illumina HT12 gene expression array data (B). Adjusted Rand Index indicates concordance in methylation and gene expression clusters. Most stable tumor grouping indicated by highest cophenetic coefficient (Coph. Coef; k = 3) with 250 genes and 10,000 methylation probes are shown.

(C) Clinical, molecular, and genotypic features of 177 primary ATRTs. Tumor subgroups determined by methylation or gene expression are indicated by red (group 1), blue (group

2A), green (group 2B) or gray (group not available) bars; clinical (tumor location, patient age, metastatic status), global patterns of CNAs (chromosomal or subchromosomal/focal), and type of *SMARCB1* alterations in individual tumors are indicated. Clinical or molecular features with significant subgroup correlation are indicated in red. *SMARCB1* alterations were classified as focal (point mutations, small indels, intergenic deletions) or broad (intragenic events, large deletions).

(D) Tumor location, median age, and age distribution in ATRT subgroups. Boxplot middle represents median, box boundaries represent first and third quartiles, and whiskers represent 10^{th} and 90^{th} percentiles.

See also Figures S2, S3, and Table S6.

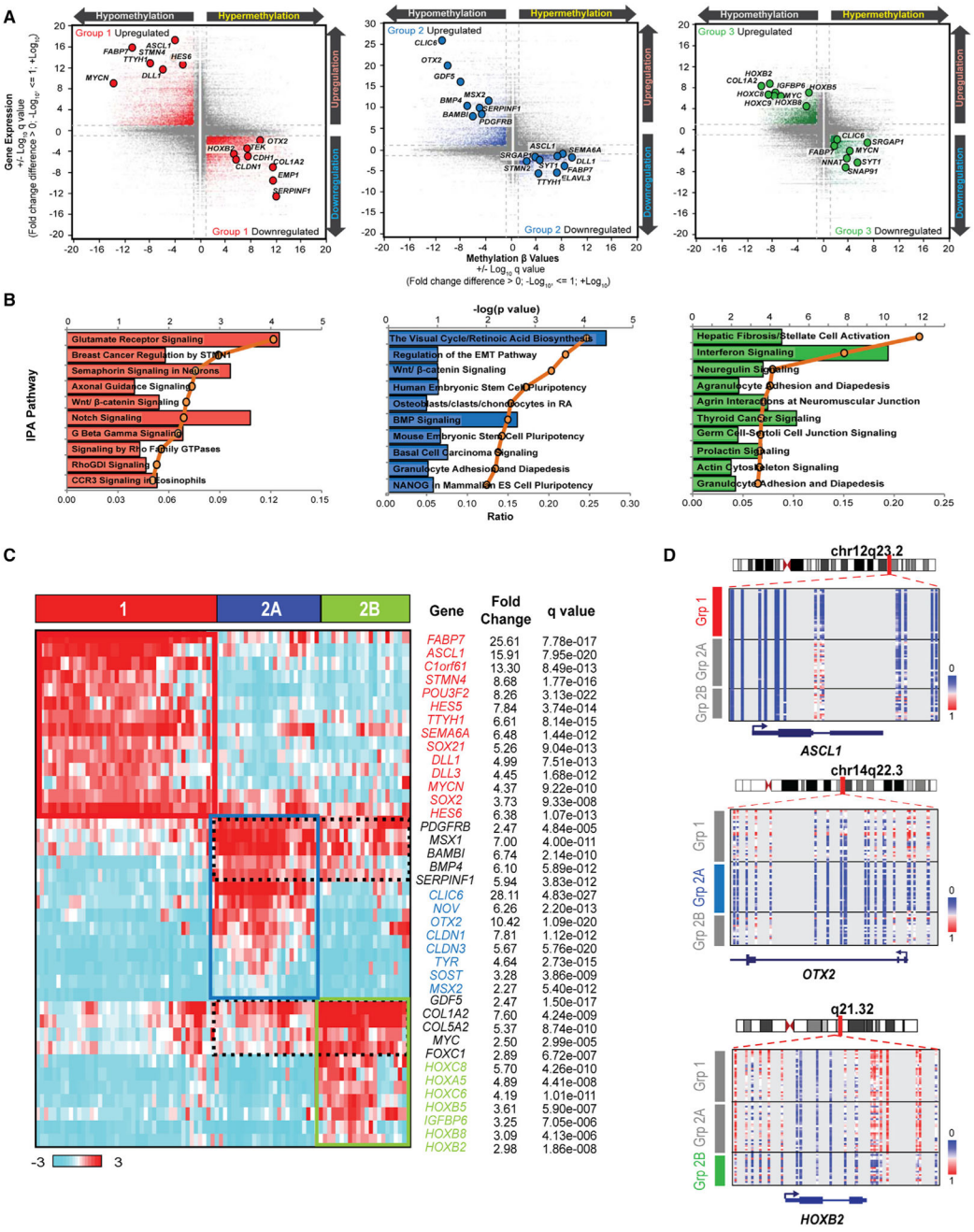

Figure 3. ATRT Subgroups have Distinct Lineage-Enriched Transcriptional and Methylation Signatures

(A) Starburst plot of ATRT subgroup-specific genes with reciprocal changes in methylation (x axis) and gene expression (y axis). Genes associated with group 1 (left panel; red), group 2A (middle panel; blue), and group 2B (right panel; green) ATRTs are highlighted.

(B) Top ten (top axis) enriched pathways for each subgroup was determined by ingenuity pathway analysis (IPA) of subgroup-specific genes with ±2-fold difference in expression; relative enrichment of pathways is shown on bottom axis.

(C) Gene expression heatmap of subgroup-enriched neural/mesenchymal lineage and NOTCH/BMP/HOX signaling genes in ATRT determined by supervised t test with FDR correction. Genes enriched in individual subgroups, or shared by subgroups 2A and 2B are shown by solid and dashed boxes, respectively.

(D) Heatmaps show methylation levels of representative lineage genes in ATRT subgroups; methylation status of probes in *ASCL1*, *OTX2*, and *HOXB2* are shown relative to transcriptional start sites.

See also Figures S4, S5, and Table S7.

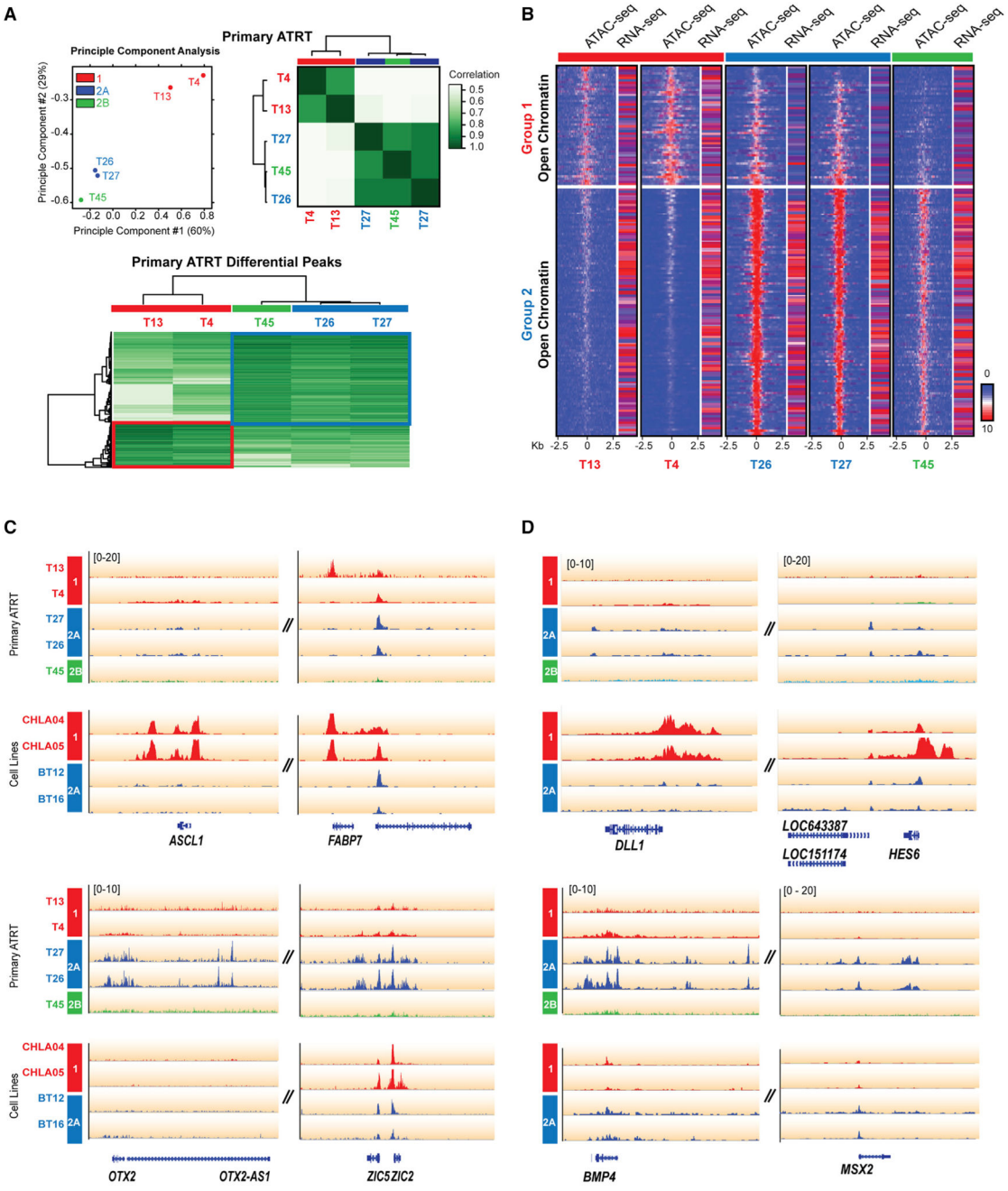

Figure 4. ATRT Subgroups Have Unique Chromatin Landscape and Functional Genomes

(A) Principle component analysis (PCA) and correlation analysis of ATAC-seq data from five primary ATRTs. Aligned sequence reads from ATAC-seq profiling were converted to peak tag counts using HOMER software for PCA and correlation analysis using DiffBind software; color gradients indicate sample relatedness. Heatmap shows peaks enriched in group 1 and 2 ATRTs.

(B) Genome-wide chromatin openness profiles of group 1 (T4, 13), 2A (T26, 27), and 2B (T45) ATRTs. Differentially open chromatin peaks (FDR < 0.5) were identified using DiffBind analysis of ATAC-seq data. Heatmap shows average read density in 20 bp bins

(range ±2.5 kb from peak center) and FPKM values of corresponding genes in individual tumors determined by RNA-seq. The color scale is proportional to read enrichment and normalized between ChIP-seq experiments relative to input DNA.
(C and D) ATAC-seq alignment tracks for subgroup-specific lineage (C) and signaling (D) genes in primary tumors and cell lines. Gene tracks are shown relative to hg19 RefSeq annotation and ATRT molecular group (red, 1; blue, 2A; green, 2B).
See also Table S8.

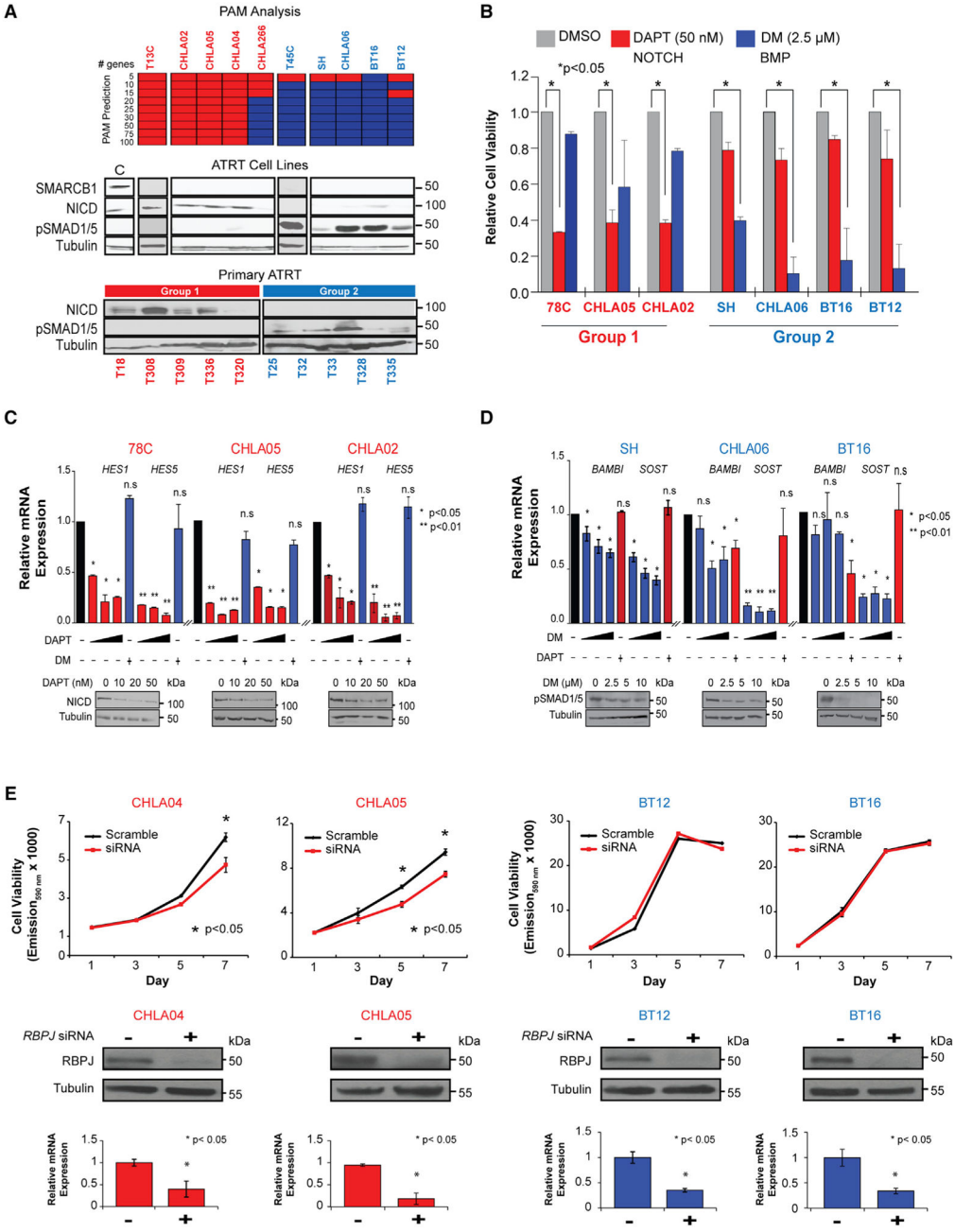

Figure 5. NOTCH and BMP Inhibitors Have Subgroup-Specific Effects on ATRT Cell Growth

(A) Molecular subtype of ten ATRT cell lines is shown with a heatmap of PAM predicted gene classifiers based on primary ATRT gene expression data and western blot analyses of NOTCH intracellular domain (NICD) and pSMAD1/5 expression in cell lines and primary tumors. UW228 medulloblastoma cell line served as a control (C) for SMARCB1 expression; tubulin served as loading control.

(B) MTS assays of group 1 and 2 cell lines respectively at 3 and 5 days post-treatment with DAPT and dorsomorphin (DM), cell viability is normalized to DMSO-treated controls.

(C and D) Effect of DAPT and DM on NOTCH and BMP signaling in ATRT cells was confirmed by qRT-PCR analyses of respective target genes and western blot analyses for NICD and pSMAD1/5 in group 1 (C) and group 2 (D) cell lines treated with increasing doses (black triangles) of DAPT or DM, and cross-treated with a single dose of DM or DAPT; ± signs indicate presence or absence of specific drugs. mRNA levels are normalized to actin, and to carrier treated controls (black bars). Significance was calculated using Student's t test.

(E) Cell viability of group 1 (CHLA04, 05) and group 2 (BT12, 16) cell lines treated with RBPJ (25 nM) and scrambled control (20 nM) siRNA were assessed using Alamar blue assays; western blot and qRT-PCR analyses confirmed RBPJ knockdown.

Error bars show ±SEM (n = 3).

See also Figure S6.

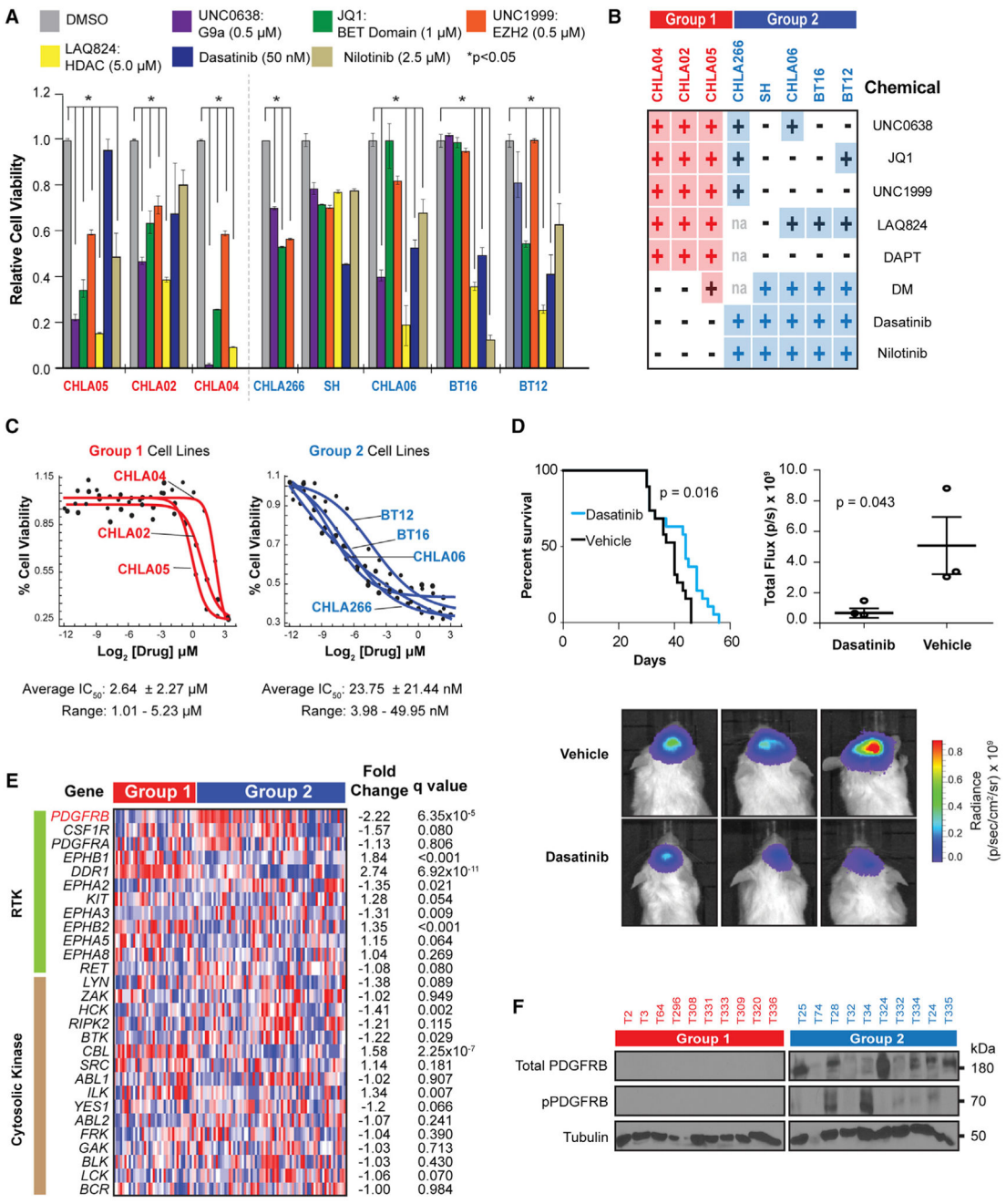

Figure 6. Subgroup-Specific Effect of Signaling and Epigenetic Pathway Inhibitors on ATRT Cell Growth

(A) Cell viability of cell lines treated with indicated small molecules for 7 days was determined by the MTS assays relative to DMSO controls over 5–7 days. Error bars show ±SEM (n = 3).

(B) Summary of MTS assays for cell lines treated with indicated chemicals. + and − indicate > or <30% reduction in cell viability, respectively.

(C) Group 1 and 2 cell lines were treated with 0.3 nM–10 μM dasatinib; IC_{50} was determined using Alamar blue assays at day 6 post-treatment.

(D) Kaplan-Meier survival analysis of mice with orthotopic BT12 cell line xenografts treated with 30 mg/kg intraperitoneal dasatinib injections for 2 weeks. Dot plot (middle bar represents mean, whiskers represent 10^{th} and 90^{th} percentiles) and BLI images depicting tumor mass at day 21 post-injection in three representative control and treated mice. Differences in survival and tumor growth were assessed using log rank (Mantel-Cox) test and ANOVA analysis, respectively.

(E) Gene expression heatmap of *PDGFRB* (red) and putative receptor (green) and cytosolic tyrosine kinase (brown) targets of dasatinib/nilotinib in ATRTs. Significance was determined by FDR adjusted Student's t test.

(F) Western blot analyses of total and pPDGFRB in primary ATRTs.

See also Figure S7.

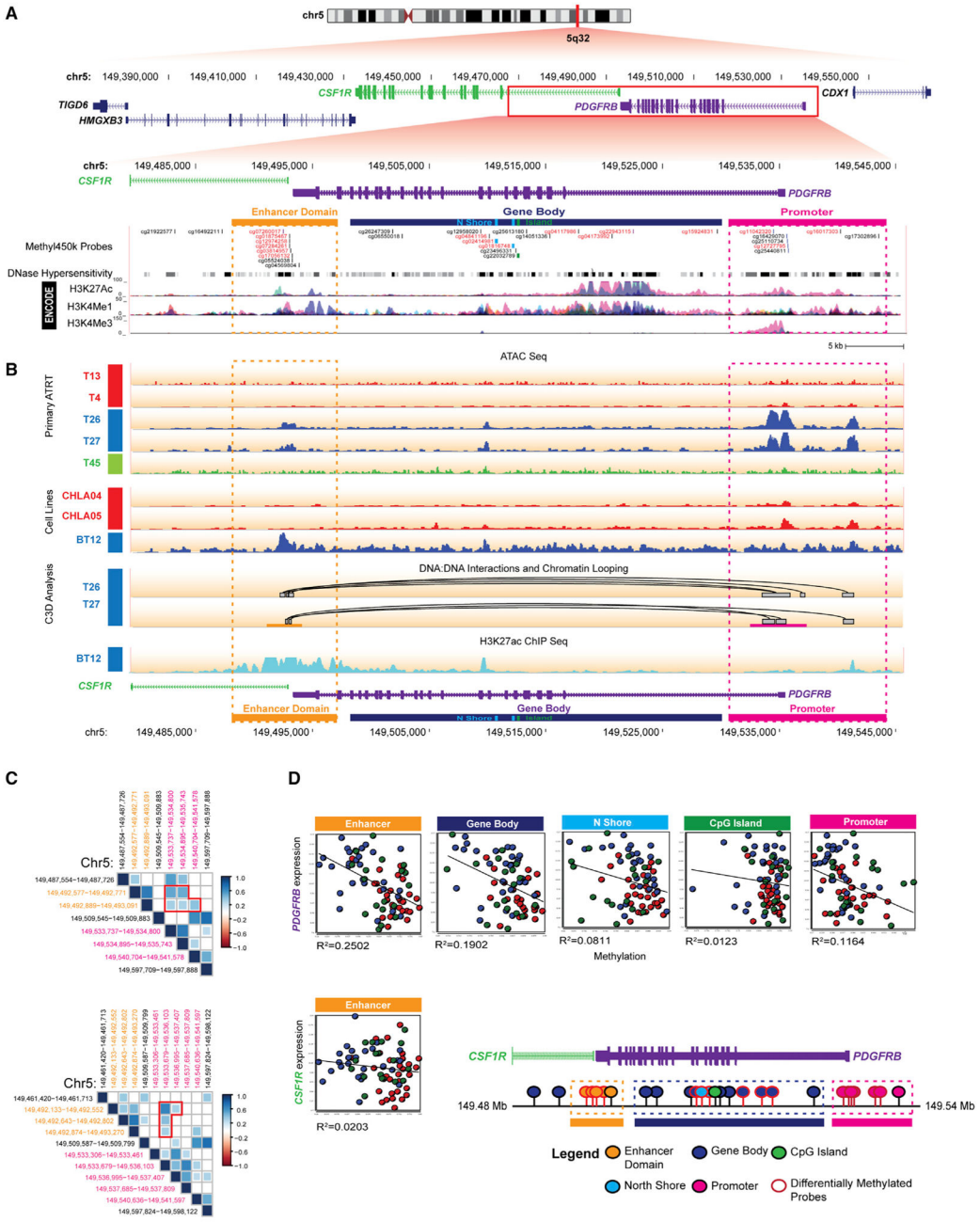

Figure 7. A PDGFRB Enhancer Element Exhibits Differential Methylation and Chromatin Association in Group 2 ATRTs

(A) Schema of *CSF1R* (green) and *PDGFRB* (purple) relative to UCSC and/or ENCODE tracks and flanking genes (chr5:149,370,252-149,566,612) with a zoomed view of putative enhancer relative to exon 1 and gene body of *CSF1R* (blue) and *PDGFRB* promoter (purple) (chr5:149,479,360-149,545,365), 450k probe locations, DNaseI hypersensitivity, and ENCODE cell line tracks for H3K27Ac, H3K4Me1, and H3K4Me3 ChIP-seq data. Probes in *PDGFRB* promoter and putative enhancer with relative hypomethylation in group 2 ATRTs is shown in red font and dashed pink and orange boxes.

(B) ATAC-seq signal for *CSF1R/PDGFRB* in primary ATRTs and cell line data is shown with C3D predicted associations (curved lines) of *PDGFRB* enhancer and promoter (boxed). Bottom track shows H3K27Ac ChIP-seq signal for BT12, a dasatinib-sensitive group 2 cell line. Group 1, 2A, and 2B primary ATRTs and cell lines are indicated in red, blue, and green, respectively.

(C) Correlation matrix of associated open chromatin regions in a 120 kb window around the *PDGFRB* promoter predicted by C3D analysis of ATAC-seq data from tumors T26 (top panel) and T27 (bottom panel). Absolute correlation is shown proportional to size of colored squares, positive and negative correlations are indicated in blue and red, respectively. All correlations were tested within a 500 kb window of *PDGFRB* promoter and adjusted for statistical significance (FDR method); blank squares indicate insignificant correlations.

(D) Pearson's correlation/linear regression analyses of *PDGFRB* and *CSF1R* gene expression (log_2, y axis) and methylation levels (β value, x axis) at the enhancer domain, *PDGFRB* gene body, North (N) shore, CpG island, and *PDGFRB* promoter. Location of differentially methylated *CSF1R-PDGFRB* probes based on 450k array data of 75 ATRTs is schematized.

See also Figure S8.

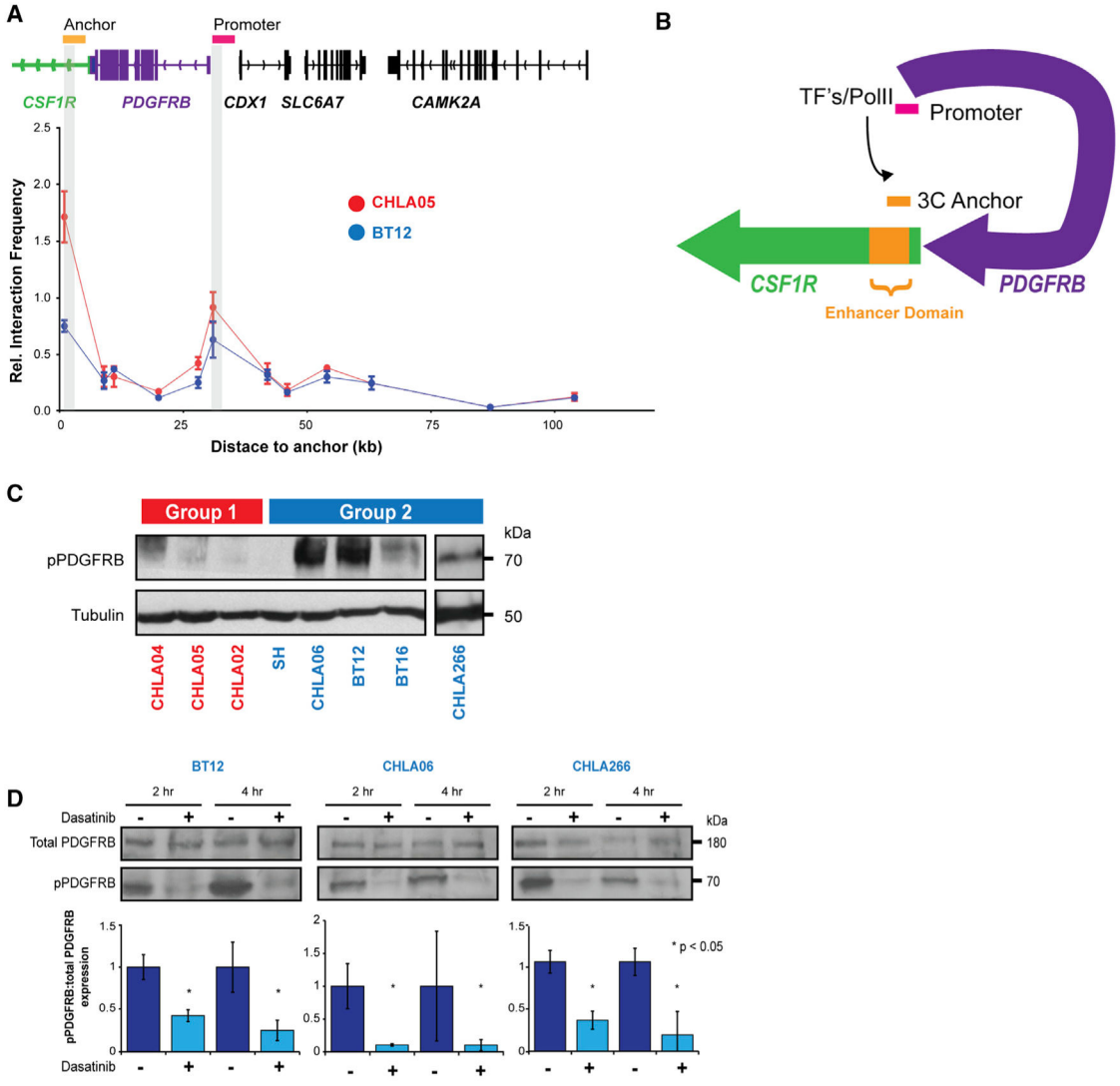

Figure 8. A Promoter-Enhancer Loop Regulates PDGFRB Expression and Confers Dasatinib/ Nilotinib Sensitivity in Group 2 ATRT

(A) 3C analyses of *PDGFRB* enhancer:promoter interaction in ATRT cell lines CHLA05 (red) and BT12 (blue). Plot indicates relative co-amplification and interaction frequency of an anchor primer in the putative enhancer with test primers located at various distances in the *CSF1R/PDGFRB* gene body and promoter (gray bars).

(B) Schema of 3C analysis indicating DNA looping and direct interaction of *PDGFRB* promoter and an enhancer 50 kb upstream.

(C) Western blot analyses of pPDGFRB expression in ATRT cell lines.

(D) Western blot and corresponding densitometric analyses of total and pPDGFRB expression in group 2 cell lines post-treatment with 50 nM of dasatinib (+) and DMSO (−). Error bars show ±SEM (n = 3).